

Supplementary Information

Extremely Enhanced Contaminants Decomposition Catalyzed by Hemin via the Coupling of Persistent Free Radicals and Ascorbic Acid

Yuyuan Yao,^{*a} Bin Jiang,^a Yajun Mao,^a Juan Chen,^a Zhenfu Huang,^a Sanqing Huang^a and Li
Zhang^b

^a National Engineering Lab of Textile Fiber Materials & Processing Technology (Zhejiang),
Zhejiang Sci-Tech University, Hangzhou 310018, China

^b The School of Material Science and Chemical Engineering, Ningbo University, Ningbo 325211,
PR China

*Corresponding author: Email: yyy0571@126.com Tel.: +86-571-86843810; Fax: +86-571-
86843255.

Experimental Section

Materials. Activated carbon fiber (ACF) was obtained from Jiangsu Sutong Carbon Fibers Co. Ltd. (Jiangsu, China). Hemin (98 wt%) was purchased from Aladdin Reagent (Shanghai, China). Reactive Red M-3BE (RR M-3BE), Acid Red 1 (AR1), Acid Orange 7 (AO7), Reactive Red X-3B (RR X-3B), Methyl Blue (MB), 8-Hydroxyquinoline (8-HQu), 4-Nitrophenol (4-NP) were used as the model contaminants without further purification. Doubly distilled water was used throughout the contaminants decomposition process. The spin trapping reagent, 5, 5-dimethyl-pyrroline-oxide (DMPO) was supplied by Tokyo Chemical Industry Co. Ltd., Tokyo, Japan. Thionylchloride, N,N'-dimethylformamide (DMF), methanol, dimethyl sulf-oxide (DMSO), dimethyl sulfone (DMSO₂), p-phenylenediamine (p-PDA), o-phenylenediamine (o-PDA), 2,3-diamino phenazine (DAPN), hydrogen peroxide (30 wt%, Sinopharm Chemical Reagent Co. Ltd., Shanghai, China) were used as analytical reagents. All other chemicals were analytical reagents.

Preparation of hemin-ACF. The hemin-ACF was obtained by immobilizing hemin on ACF based on the consideration that hemin had a conjugated π -electron system similar to that of ACF, which could promote a facile pathway for electron transfer between hemin and ACF, thus it's beneficial for us to understand the electronic interaction between hemin and ACF. The hemin-ACF was prepared according to our previously report.¹

Experimental procedure. The catalytic oxidation of various contaminants were carried out in a 40-mL glass beaker while controlling the temperature at 50 °C using a constant temperature shaker water bath (SHA-B, Guowang Laboratorial Equipment Factory, China). A typical reaction mixture contained the following initial concentrations: (a) dye (50 μ M, 20 mL); (b) supported catalyst hemin-ACF (10 g/L, containing 169 μ M hemin) or hemin (169 μ M) with or without AA

(3mM); (c) oxidant H₂O₂ (50 mM). The values of apparent rate constant k_{obs} for the catalytic reaction can be obtained from the slope of the plot of $\ln(C_t/C_0)$ versus time. Electron paramagnetic resonance (EPR) signals of radicals were recorded at ambient temperature using a Bruker A300 spectrometer (Germany). The settings for the EPR spectrometer were as follows: center field, 3518 G; microwave frequency, 9.77 GHz; modulation frequency, 100 kHz; power, 20.00 mW. Before the EPR test, the solid samples (hemin, hemin-ACF) were collected and dried under vacuum.

Decomposition rate

The decomposition rate can be represented as follows:

$$\text{The residual of dyes} = C_t/C_0 * 100\% = A_t/A_0 * 100\%;$$

where C_0 is the initial concentration of target dyes and C_t is the actual concentration of target dyes after reaction time t , and A_0 is the initial absorbance of target dyes and A_t is the absorbance of target dyes after reaction time t .

Discussion

EPR spectrum of ACF. As depicted in Fig. S1, EPR spectrum of ACF was acquired, a narrow singlet signal devoid of hyperfine structure located at 3513G was observed for the ACF, with an EPR g-factor of 2.0037. This signal remained almost unchanged for several days, which was consistent with the literature report^{2,3} and indicated that ACF contained persistent free radicals (PFRs). These PFRs could be carbon-centered radicals with adjacent oxygen atom, based on the report that the g factors for carbon-centered radicals were less than 2.0030, and those for carbon-centered radicals with an adjacent oxygen atom were in the range of 2.0030-2.0040, while oxygen-centered radicals had g-factors larger than 2.0040.^{4,5}

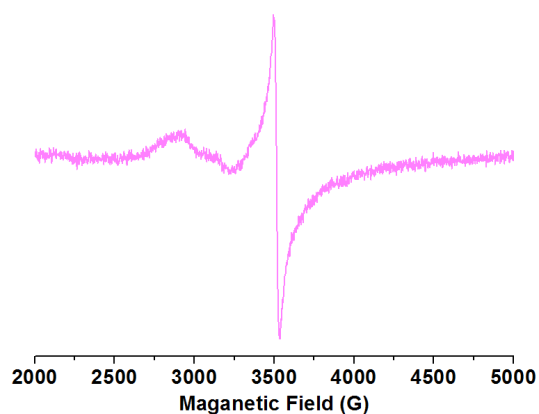


Fig. S1. EPR spectrum of ACF at room temperature.

Conversion of hemin(Fe^{III}) to hemin(Fe^{II})

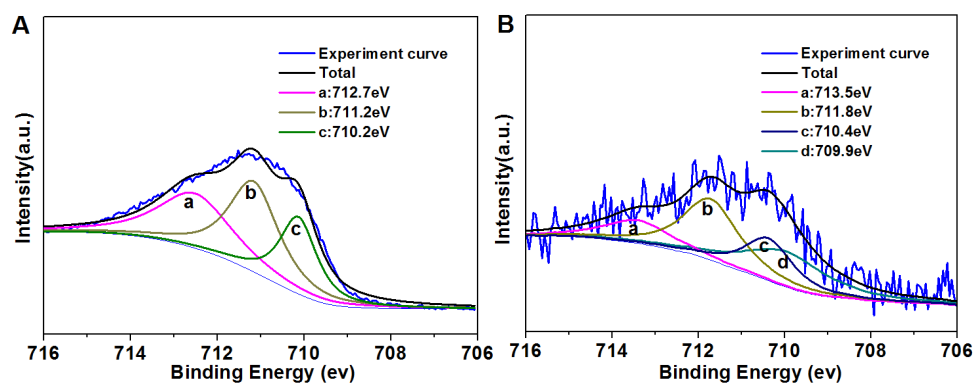


Fig.S2. Fe_{2p} XPS spectra of (A) hemin and (B) hemin-ACF.

The effect of AA on the PFRs after cyclic utilizations

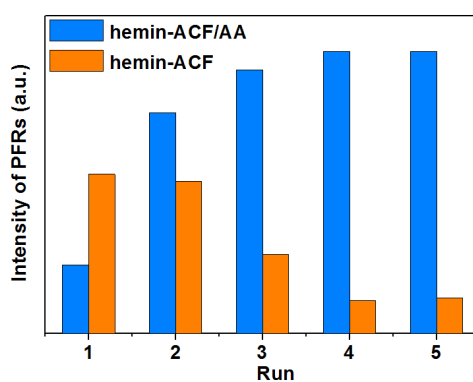


Fig. S3. Intensity of PFRs in the hemin-ACF (located at 3513G) after cyclic utilizations in the hemin-ACF/ H_2O_2 and hemin-ACF/AA/ H_2O_2 systems, respectively. Conditions: [hemin-ACF]=10 g/L (containing 169 μM hemin), [H_2O_2]=50 mM, [AA]=3 mM, initial pH 7.3, at 50 $^\circ\text{C}$, reaction time for every run: 60 min.

Pathway of the formation of •R. The possible pathway of the formation of carbon-based radicals derived from the decomposition of AA in the hemin-ACF/AA/H₂O₂ system was illustrated in Fig. S4. AA was firstly oxidized to dehydroascorbic acid (DHA), and major DHA decomposition products were 2,3-diketogulonic acid (2,3-DKG), which could further decomposed into L-threo-pentos-2-ulose (L-xylosone) and 3,4-dihydroxy-2-oxobutanal (L-threosone). The L-threosone could be converted to DL-glyceraldehyde, which was further attacked by •OH to form glyceraldehyde radicals. And the glyceraldehyde radicals could convert to glycolaldehyde, which reacted with •OH to generate glycolaldehyde radicals.

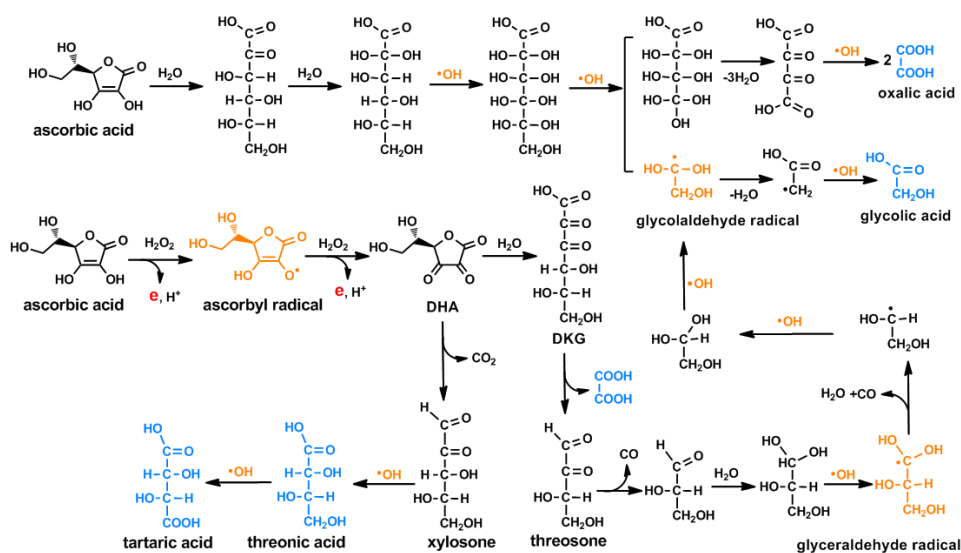


Fig. S4. Possible pathway of the formation of carbon-based radicals derived from the decomposition of AA in the hemin-ACF/AA/H₂O₂ system. The blue substances were detected by GC-MS, the orange substances were detected by EPR.

Detection of hemin ($\text{Fe}^{\text{IV}}=\text{O}$) and detailed conditions for Fig. 2. Dimethyl sulfoxide (DMSO) was employed as a probe compound for high valent $\text{Fe}^{\text{IV}}=\text{O}$.^{6,7} As shown in Fig. 2B and S5, in the presence of H_2O_2 alone, the UV/Vis spectrum of DMSO remained almost unchanged, indicating that DMSO was not oxidized by sole H_2O_2 , while in the hemin-involved systems, significant enhancement of the peak at 197nm and 207 nm (Fig. 3B, curves a, b, c and d) was attributed to the generation of dimethyl sulfone (DMSO_2), demonstrating that a high valent hemin ($\text{Fe}^{\text{IV}}=\text{O}$) was formed and the hemin ($\text{Fe}^{\text{IV}}=\text{O}$) production was ranked in the order of hemin<hemin/AA<hemin-ACF<hemin-ACF/AA. The experimental conditions for Fig. 2B and S5 were as follows: [hemin]=169 μM , [hemin-ACF]=10 g/L (containing 169 μM hemin), [DMSO]=1 mM, [H_2O_2]=20 μM , [AA]=8 μM , initial pH 7.3, after 10 min of reaction at ambient temperature. To quantitatively analyze the high valent hemin($\text{Fe}^{\text{IV}}=\text{O}$) formation, the relative amounts of hemin($\text{Fe}^{\text{IV}}=\text{O}$) in different systems were calculated according to the absorbance difference between hemin-involved species (hemin, hemin/AA, hemin-ACF and hemin-ACF/AA) and DMSO at 197nm, as shown in Fig. 2D. The conditions for Fig. 2A and 2C: [hemin]=169 μM , [hemin-ACF]=10 g/L (containing 169 μM hemin), [H_2O_2]=50 mM, [AA]=3 mM, [DMPO]=5 mM, at 50 °C, initial pH 7.3.

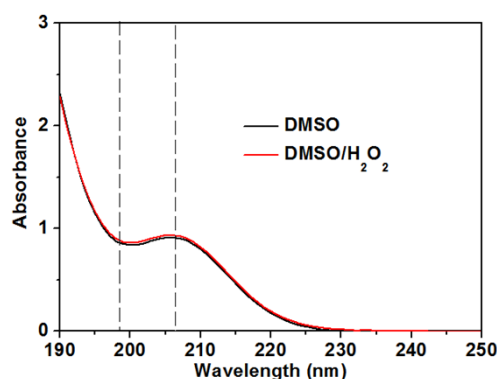


Fig. S5. UV/Vis spectroscopy of DMSO and oxidation products of DMSO by H_2O_2 .

Catalytic decomposition of different organic pollutants. To further testify whether the synergistic effect of PFRs (ACF) and AA was applicable for other contaminants, several aromatic compounds including Acid Red 1 (AR1), Acid orange 7 (AO7), Reactive Red X-3B (RR X-3B), Methyl Blue (MB), 8-Hydroxyquinoline (8-HQu) and 4-Nitrophenol (4-NP) were selected as other contaminants for the oxidation reaction, we found similar extreme rate acceleration of contaminants oxidative transformation by the hemin-ACF/AA/H₂O₂ system. As listed in Table S1, hemin alone could only catalyze less than 1.5 % of oxidation of aromatic compounds (initial 50 μ M) within 2 min, while either the introduction of ACF or AA to the hemin/H₂O₂ system promoted the catalytic efficiency of hemin to some extent of around 6 % to 69.7 %. When AA was introduced to the hemin-ACF/H₂O₂ system, we surprisingly found that more than 95 % of aromatic compounds (except 81 % for 8-HQ and 83.7 % for 4-NP) were oxidized within 2 min accompanying with a decomposition rate constant hundreds or even thousands of times that in the hemin/H₂O₂ system and several or dozens of times that in the hemin/AA/H₂O₂ system and hemin-ACF/H₂O₂ system.

Table S1. Comparison of decomposition rates for different organic pollutants by hemin/H₂O₂, hemin/AA/H₂O₂, hemin-ACF/H₂O₂ and hemin-ACF/AA/H₂O₂, respectively^a.

Entry	Contamin.	Initial conc. (μ M)	Cat. ^b	Conversion (%)		k_{obs} (10^{-3} min^{-1})
				within 1 min	within 2 min	
1	AR1	50	A	0.8	1.2	1.7
			B	4.9	10.4	41.9
			C	8.5	16.7	79.9
			D	95.6	98.4	3347.1

2	AO7	50	A	0.3	0.3	1.9
			B	4.3	9.0	68.5
			C	16.2	25.9	191.8
			D	61.1	95.2	1427.5
3	RR X-3B	50	A	0.6	0.6	4.5
			B	8.3	16.9	69.7
			C	8.8	19.1	95.6
			D	82.4	97.8	1865.7
4	MB	50	A	0.3	0.5	4.4
			B	0.9	6.0	58.5
			C	14.1	29.4	327.3
			D	75.8	97.4	1737.6
5	8-HQu	500	A	0.3	0.7	0.9
			B	14.0	15.6	14.9
			C	57.2	69.7	436.8
			D	72.2	81.0	595.2
6	4-NP	250	A	0.3	0.5	1.5
			B	4.7	6.8	28.0
			C	18.2	44.4	390.5
			D	66.3	83.7	700.9

^aStandard conditions: [hemin]=169 μ M, [hemin-ACF]=10 g/L (containing 169 μ M hemin), [H₂O₂]=50 mM, [AA]=3 mM, at 50 °C, initial pH 7.3. ^bA, B, C and D represent hemin/H₂O₂, hemin/AA/H₂O₂, hemin-ACF/H₂O₂ and hemin-ACF/AA/H₂O₂, respectively.

Eliminating the interference of the pH, adsorption and decomposition products of AA. To explain this large enhancing effect of PFRs (ACF) coupled with AA in the hemin-ACF/AA/H₂O₂ system, some influencing factors such as pH value, adsorption, and decomposition products of AA should be considered in priority. During the experiments, we found that the addition of AA obviously decreased the initial pH value of RR M-3BE solution to some degree (7.3 to 3.5). It is known that the catalytic activity of hemin and hemin-ACF are strongly related to the pH of the solution.⁸ We therefore monitored the pH changes in the hemin/H₂O₂, hemin-ACF/H₂O₂, AA/H₂O₂, hemin/AA/H₂O₂, hemin-ACF/AA/H₂O₂ systems and found the pH values of the solution decreased (Fig. S6A, 7.3 to 4.7 for the hemin/H₂O₂ system; 7.3 to 3.5 for the hemin-ACF/H₂O₂ system; 3.5 to 3.0 for the AA/H₂O₂ system; 3.5 to 3.0 for the hemin/AA system; 3.5 to 3.0 for the hemin-ACF/AA system). As the addition of buffer solutions would inhibit the RR M-3BE decomposition in the four systems, to check the influence of different initial pH values on the RR M-3BE decomposition performances of four systems, we conducted the decomposition experiments at the same pH values by adjusting the initial pH values of the four systems to 3.5 with HClO₄ and NaOH before the RR M-3BE decomposition and found the RR M-3BE decomposition trends in the four systems were similar to that of Fig. 3 (Fig. S6B). The influence of initial pH values on the RR M-3BE decomposition in the hemin-ACF/AA/H₂O₂ system was also investigated (Fig. S6C). We found that the pH value variation in the range of 3.0 to 7.3 only slightly changed the RR M-3BE decomposition rate, indicating that the lower initial pH decrease (in the range of 3.0 to 7.3) caused by the addition of AA did not mainly account for the extremely enhanced decomposition of RR M-3BE. Moreover, the pH value variation in the range of 3.5 to 9.0 almost did not change the RR M-3BE decomposition rate in the hemin-ACF/AA/H₂O₂ system

(Fig. S6D), suggesting that the hemin-ACF/AA/H₂O₂ system could efficiently degrade RR M-3BE in a wide working pH range.

Since the addition of AA also influenced the adsorption of hemin-ACF to RR M-3BE in addition to the variation of initial pH values, we investigated the effect of AA on the adsorption of hemin-ACF to RR M-3BE and found the RR M-3BE removal by adsorption only increased 12.02% (from 27.76% to 39.78%) with the addition of 3 mM AA and 15.95% (from 27.76% to 43.71%) even with the addition of 50 mM AA (Fig. S7). This finding indicated that the adsorption improvement of hemin-ACF to RR M-3BE was also not the main reason for the extreme RR M-3BE decomposition enhancement.

As AA itself acted as an organic compound reacted competitively with ROS, consuming ROS species available for the RR M-3BE decomposition, AA itself was rapidly decomposed in the hemin-ACF/H₂O₂ system accompanying the RR M-3BE removal. It was of interest to testify the possibility that highly active intermediates might exist in the decomposition products of AA, causing the extreme acceleration of RR M-3BE decomposition. Gas chromatography-mass spectrometer (GC-MS) was used to detect the decomposition products of AA in the hemin-ACF/AA/H₂O₂ system and found that several aliphatic acids were formed during the simultaneous decomposition of AA in the hemin-ACF/H₂O₂ system, and the main intermediates were proved to be oxalic acid, tartaric acid, glycolic acid, and threonic acid (Fig. S8-S12 and Table S2). However, when 3 mM oxalic acid, tartaric acid, glycolic acid, and threonic acid were added into the hemin-ACF/AA/H₂O₂ system, the removal of RR M-3BE was obviously decreased by 25.3%, 40.3%, 5.9%, and 19.9%, respectively (Fig. S13). Thus, the decomposition products of AA in the hemin-

ACF/AA/H₂O₂ system was not responsible for the dramatically enhanced decomposition of RR M-3BE.

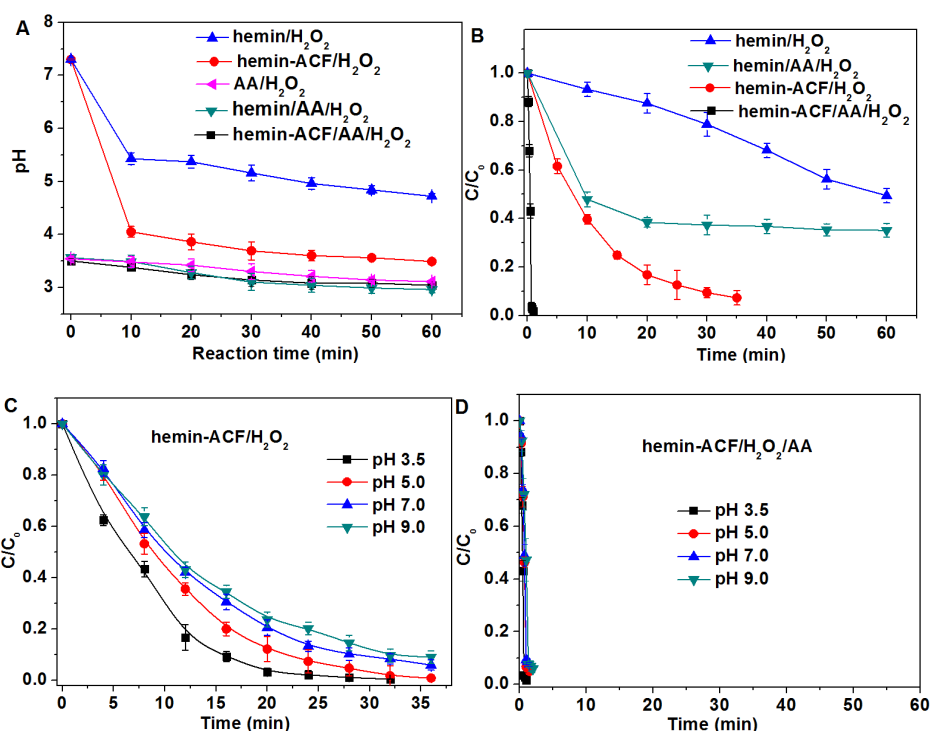


Fig. S6. (A) The temporal pH values of RR M-3BE solution as a function of time during the aerobic; (B) Time profiles of the RR M-3BE decomposition in different systems at pH 3.5; (C) Time profiles of the RR M-3BE decomposition in hemin-ACF/H₂O₂ systems at different initial pH values; (D) Time profiles of the RR M-3BE decomposition in hemin-ACF/AA/H₂O₂ systems at different initial pH values.

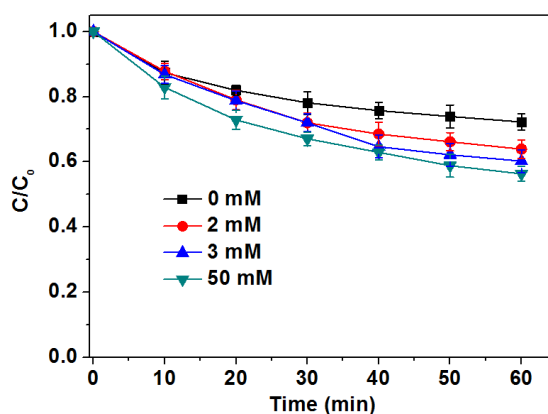


Fig. S7. Effect of AA concentration on the adsorption of hemin-ACF to RR M-3BE.

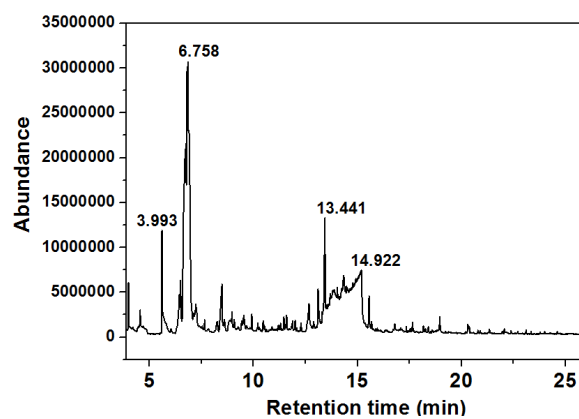
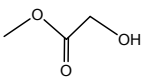
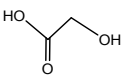
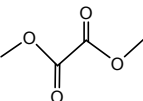
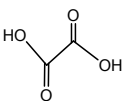
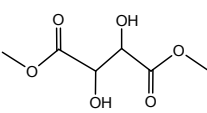
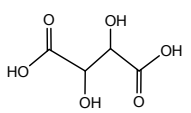
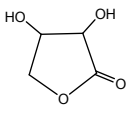
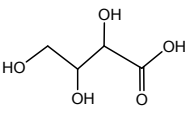


Fig. S8. The total ion current (TIC) diagrams of GC-MS for products in the systems of hemin-ACF/AA/H₂O₂.

Table S2. Identification of the decomposition products of AA in the hemin-ACF/H₂O₂ system after reaction for 1 min by GC-MS.

Entry	Time (min)	The detected products	Main products
1	3.993		
2	6.758		
3	13.441		
4	14.922		

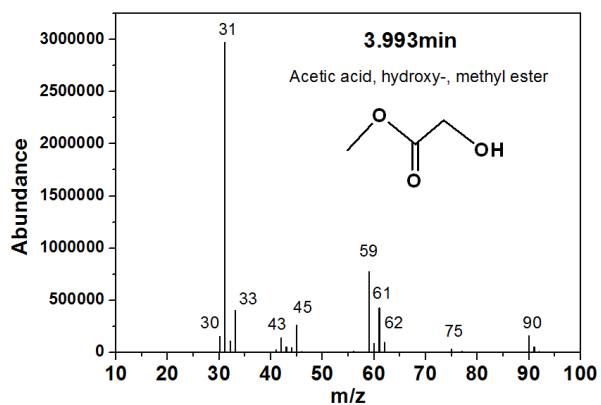


Fig. S9. Mass spectrum of compound at retention time 3.993 min in TIC (Fig. S8) corresponding to Acetic acid, hydroxy-, methyl ester.

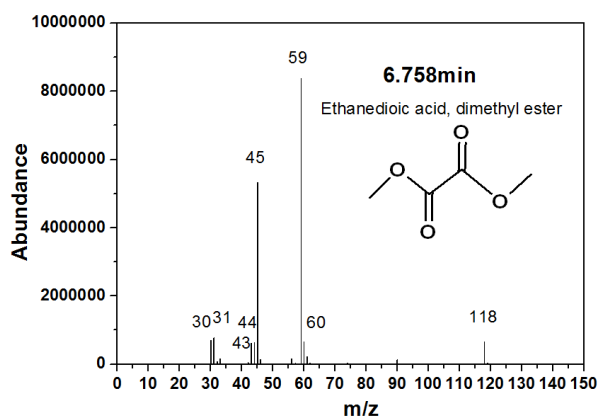


Fig. S10. Mass spectrum of compound at retention time 6.785 min in TIC (Fig. S8) corresponding to Ethanedioic acid, dimethyl ester.

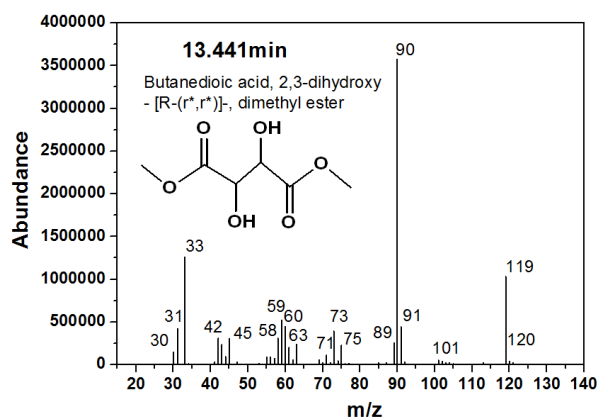


Fig. S11. Mass spectrum of compound at retention time 13.441 min in TIC (Fig. S8) corresponding to Butanedioic acid, 2, 3-dihydroxy-[R-(r*, r*)]-, dimethyl ester.

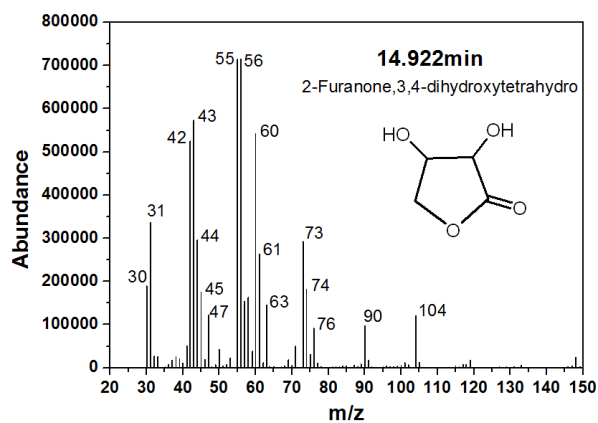


Fig. S12. Mass spectrum of compound at retention time 13.441 min in TIC (Fig. S8) corresponding to 2-Furanone, 3, 4-dihydroxytetrahydro.

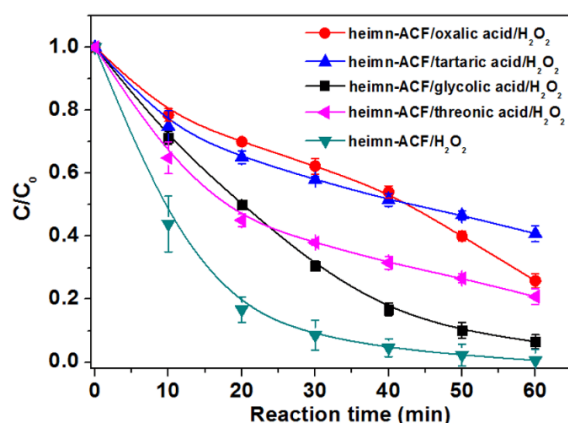


Fig. S13. Effect of AA decomposition products on the RR M-3BE decomposition in hemin-ACF/H₂O₂ systems.

The role of •R in the enhanced decomposition. It has reported that carbon-based radicals were involved in many mechanisms of DNA damage.⁹ Preliminary results suggest that these carbon radicals do indeed cause single strand breaks in pBR322 DNA.¹¹ Therefore, these carbon-based radicals might attack the contaminants, resulting in their decomposition. To further testify whether these carbon-based radicals were responsible for the enhanced decomposition, designed experiments were carried out. As monosaccharides such as DL-glyceraldehyde could be autoxidized by buffer ions to produce carbon-based radicals, which was the same as that in the hemin-ACF/AA/H₂O₂ system, 3 mM monosaccharide was incubated for 10 min in 100 mM sodium phosphate (pH 7.4) at 50 °C, and a same sextet signal with hyperfine coupling parameters ($\alpha_H=22.8$ G, $\alpha_N=15.8$ G) occurred as shown in Fig. S14. Whereas when 50 μ M RR M-3BE was present, only 15.2 % of dye decomposition were observed during the autoxidation of DL-glyceraldehyde. This results indicated that these carbon-based radicals were not mainly responsible for the enhanced decomposition. Combined with other results mentioned above, it can be concluded the •OH and hemin(Fe^{IV}=O) were mainly responsible for the enhanced decomposition.

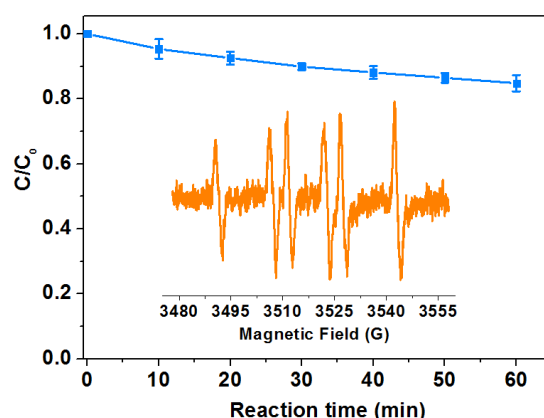


Fig. S14. Time profiles of RR M-3BE decomposition in the system of DL-glyceraldehyde/sodium phosphate. Conditions: [RR M-3BE]=50 μ M, [DL-glyceraldehyde]=3 mM, [sodium phosphate

(pH 7.4)] = 100 mM, 50 °C. The inset shows spin-trapped intermediates from DL-glyceraldehyde autoxidation at pH 7.4 and 50 °C. Reaction mixtures contained 3 mM DL-glyceraldehyde in 100 mM sodium phosphate buffer (pH 7.4) and 50 °C, with 10 mM DMPO.

The electron transfer from ACF to H₂O₂. We checked the EPR spectrum of the ACF/H₂O₂ system and found that the PFRs in ACF decreased obviously accompanying with the generation of •OH during the reaction process (Fig. S15 and S16), indicating an electron transfer occurred from ACF to H₂O₂. However, the process was not the main factor responsible for the enhancement of organic pollutant decomposition based on the fact that ACF/H₂O₂ could not efficiently remove the RR M-3BE (Fig. S17).

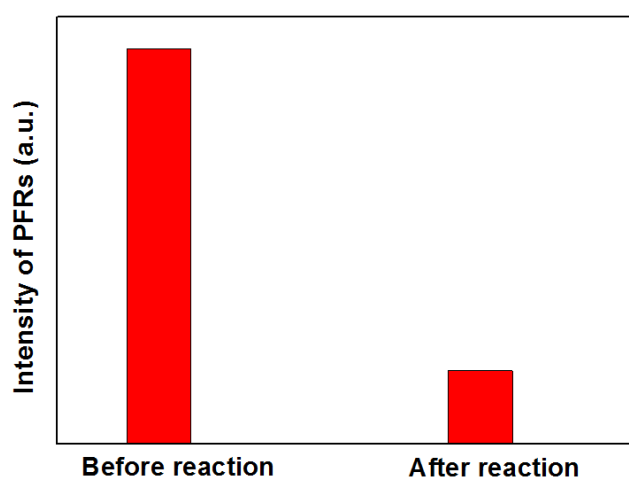


Fig. S15. Intensity of PFRs in ACF in the ACF/H₂O₂ system. Conditions: [ACF]=10 g/L, [H₂O₂]=50 mM, initial pH 7.3, at 50 °C, reaction time: 60 min.

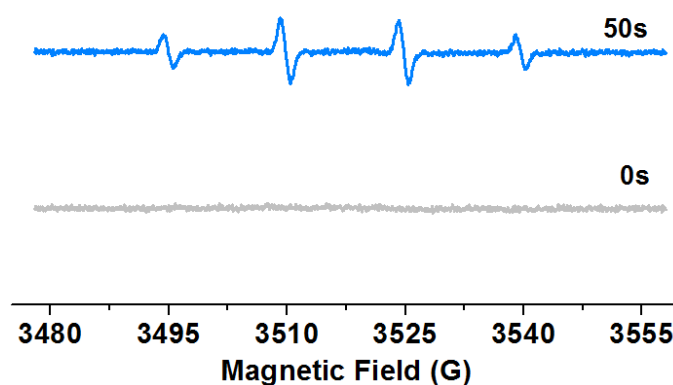


Fig. S16. DMPO-trapping EPR spectra in ultra-pure water solutions in the presence of ACF (10 g/L) with H₂O₂ (50 mM) and DMPO (10 mM).

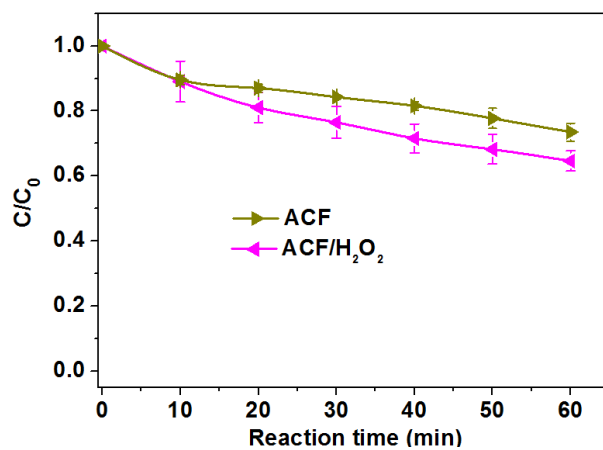


Fig. S17. Time profiles of RR M-3BE removal in the systems of ACF and ACF/ H_2O_2 . Conditions:

[RR M-3BE]=50 M, [H_2O_2]=50 mM, [ACF]=10 g/L at pH 7.3, T=50 °C.

Influencing factors on the ROS generation and dye decomposition. The amounts and types of ROS in the hemin-ACF/AA/H₂O₂ system was also influenced by reaction conditions, such as hemin-ACF dosage, H₂O₂ concentration, and AA concentration. Fig. S18 illustrates the effect of hemin-ACF dosage on the RR M-3BE decomposition in the hemin-ACF/AA/H₂O₂ system. In the presence of 0.25 g/L hemin-ACF, 3 mM AA, and 50 mM H₂O₂, a weak intensity of DMPO-•OH adducts and DMPO-•Asc⁻ adducts occurred and the RR M-3BE was completely removed in 10 min. As the catalyst dosage increased to 2.5 g/L, the sextet signal of DMPO-•R adducts appeared, which greatly accelerated the decomposition rate and reduced the decomposition time to 2 min. When the catalyst dosage further increased to 15 g/L, the intensity of DMPO-•OH adducts and DMPO-•R adducts drastically increased and the DMPO-•Asc⁻ adducts disappeared, leading to a rapidly removal of RR M-3BE in 1min.

AA concentration is another important factor influencing the catalytic ability of hemin-ACF. As shown in Fig. S19, in the presence of 2 mM AA, 10 g/L hemin-ACF and 50 mM H₂O₂, a strong intensity of DMPO-•OH adducts and DMPO-•R adducts occurred and the decomposition of RR M-3BE was completed in 20 min. When the AA concentration increased to 10 mM, although the intensity of DMPO-•OH adducts and DMPO-•R adducts decreased, a new sextet signal with hyperfine coupling parameters ($\alpha_{\text{H}}=18.7$ G, $\alpha_{\text{N}}=15.6$ G) assigned to the DMPO-CO₂•⁻ adducts¹⁰ occurred, obviously speeding the reaction rate and completely removing the RR M-3BE in 1 min. When the AA concentration further increased to 50 mM, excess radicals could be terminated by radicals coupling reaction and be scavenged by AA, which produced •Asc⁻. Hence, the EPR spectra in the presence of 50 mM AA only exhibited the DMPO-•Asc⁻ adducts and the RR M-3BE was rapidly degraded in 1 min.

Fig. S20 represents the effect of H_2O_2 concentration on the decomposition of RR M-3BE. In the presence of 25 mM H_2O_2 , 3 mM AA, and 10 g/L hemin-ACF, the EPR spectra exhibited characteristic peaks of DMPO- $\bullet OH$ adducts, DMPO- $\bullet R$ adducts and oxidized DMPO nitroxide metabolite. And the maximum intensity of DMPO- $\bullet OH$ adducts was almost equal to that of the DMPO- $\bullet R$ adducts. When the H_2O_2 concentration increased to 50 mM, although the intensity of DMPO- $\bullet OH$ adducts and DMPO- $\bullet R$ adducts increased, the relative intensity of DMPO- $\bullet OH$ adducts with respect to DMPO- $\bullet R$ adducts decreased. It might be attributed to that the $\bullet OH$ further reacted with the decomposition intermediates of AA to produce $\bullet R$, thus the $\bullet OH$ decreased and the $\bullet R$ increased relatively. When the H_2O_2 concentration increased to 100 mM, the DMPO- $\bullet OH$ adducts and DMPO- $\bullet R$ adducts further increased. And the catalytic decomposition rate increased with the increase of the H_2O_2 concentration from 25 to 100 mM.

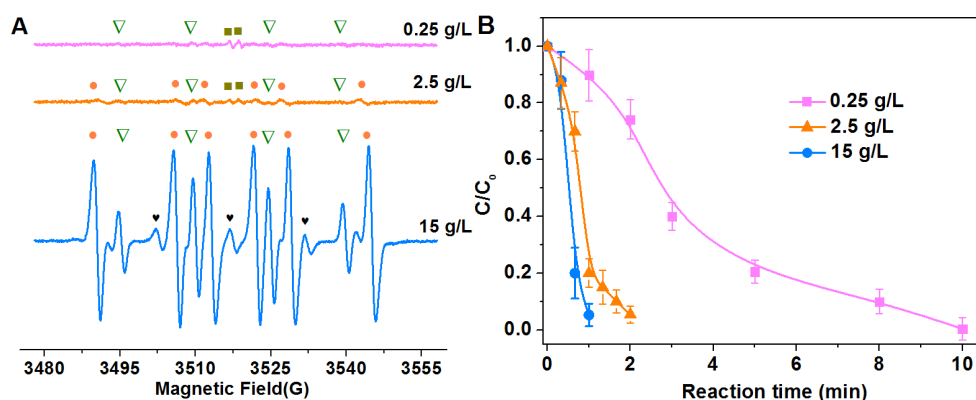


Fig. S18. The effect of hemin-ACF dosage on the catalytic decomposition of RR M-3BE. ▽: hydroxyl radicals; ●: carbon-based radicals; ■: ascorbyl radicals; ♥: oxidized DMPO nitroxide metabolite ($\alpha_N=15.0$ G).

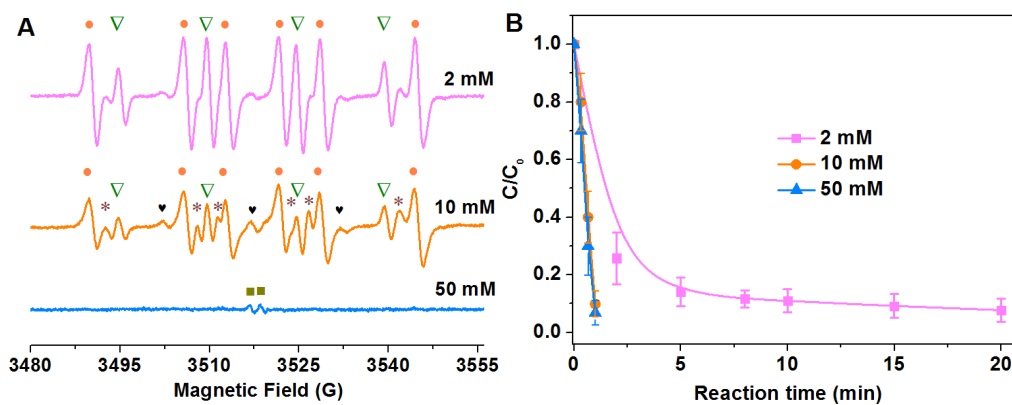


Fig. S19. The effect of AA concentration on the catalytic decomposition of RR M-3BE. ∇ : hydroxyl radicals; \bullet : carbon-based radicals; \blacksquare : ascorbyl radicals; $*$: carbon dioxide radicals; \heartsuit : oxidized DMPO nitroxide metabolite ($\alpha_N=15.0$ G).

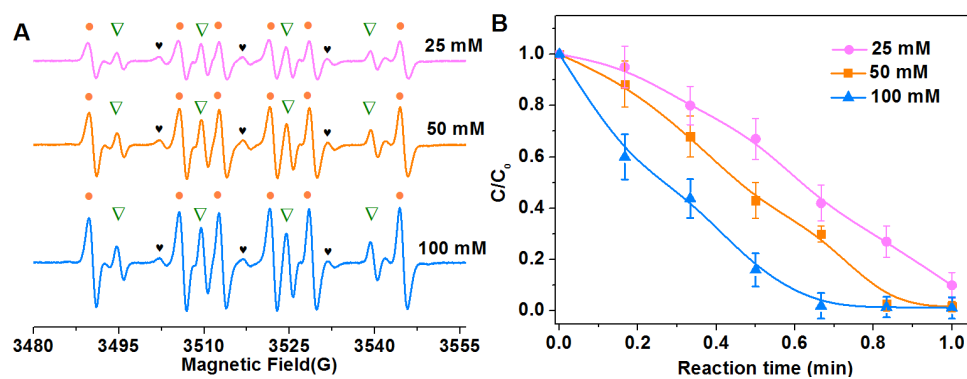


Fig. S20. The effect of H_2O_2 concentration on the catalytic decomposition of RR M-3BE. ∇ : hydroxyl radicals; \bullet : carbon-based radicals; \heartsuit : oxidized DMPO nitroxide metabolite ($\alpha_N=15.0$ G).

Mechanism for extremely enhanced decomposition from the perspective of structure change of hemin-ACF during the catalytic process. To further reveal the mechanism for extremely enhanced decomposition of organic contaminants in the hemin-ACF/AA/H₂O₂ system, XPS experiments were carried out to demonstrate the change of structure of hemin-ACF after utilization. As shown in Fig. S21, for the fresh hemin-ACF, the O 1s peaks at 531.6 eV and at 532.8 eV were assigned to oxygen in a C=O double bond and oxygen in a single bond of the hydroxyl group (–O–H), respectively. However, after recycle utilization, the intensity of –O–H peaks for hemin-ACF decreased obviously accompanying by an increase of the intensity of C=O peaks, suggesting a conversion of C–O–H to C=O. When AA was introduced to the hemin-ACF/H₂O₂ system, the intensity of –O–H peaks increased slightly, suggesting a converse transformation of C=O to C–O–H. Consequently, the proposed mechanism for the dramatically enhanced decomposition in the hemin-ACF/AA/H₂O₂ system was depicted in Scheme S1 (Eqs 1-8).

Activated carbon fiber is an effective reducing agent for many high oxidation state ions such as Au^{III}, Hg^{II}, Pt^{IV} and Fe^{III}.^{12,13} M. Uchida et al. reported that ACF could reduce Fe^{III} to Fe^{II} due to its hydrophilic groups such as phenolic hydroxyl group.¹⁴ J. S LaKind et al. reported that Fe^{III} could be reduced to Fe^{II} by phenols.¹⁵ Therefore, in the hemin-ACF/H₂O₂ system, the phenol moieties in ACF could transfer electrons to hemin(Fe^{III}), resulting in the formation of PFRs in hemin-ACF and hemin(Fe^{II}) (eq 1) (The reduction of hemin(Fe^{III}) to hemin(Fe^{II}) was evidenced by XPS experiments shown in Fig. S2). And the PFRs further reduced the hemin(Fe^{III}) to hemin(Fe^{II}), while itself was converted to quinone (eq 2). These reactions in eqs 1 and 2 could explain the decrease of intensity of –O–H peaks and increase of intensity of C=O peaks in the recycle hemin-

ACF in the hemin-ACF/H₂O₂ system, as shown in Fig. S21A and S21B. When AA was introduced to the hemin-ACF/H₂O₂ system, the quinone moieties in ACF could get electrons from AA to generate semiquinone type PFRs (eq 3), which explained the increase of the intensity of PFRs located in 3513G with the addition of AA, as shown in Fig. 1B and 2. Meanwhile, the quinone moieties in ACF could be converted to phenol moieties (eq 3), which was in good agreement with the increase of intensity of hydroxyl group (-O-H) in recycle hemin-ACF in the hemin-ACF/AA/H₂O₂ system as shown in Fig. S21C. These PFRs could also directly transfer electrons to H₂O₂ to generate •OH (eq 4), which was evidenced by Fig. S19 and consistent with the report by G. Fang.¹⁶ The hemin(Fe^{II}) and hemin(Fe^{III}) could catalytically decompose H₂O₂ to produce •OH while themselves were converted to hemin(Fe^{III}) and hemin(Fe^{IV}=O). These generated •OH and hemin(Fe^{IV}=O) rapidly broke down the molecules of aromatic contaminants to decomposed products. In summary, Eqs 1 and 2 accelerated the recycling of hemin(Fe^{II}) from hemin(Fe^{III}), which dominated •OH production. Eqs 3 regenerated the PFRs formation, promoting the electron transfer from PFRs to hemin and H₂O₂ to produce •OH. Eq 4 directly contributed to the decomposition of H₂O₂ to •OH. Eqs 5 and 6 showed that hemin(Fe^{II}) and hemin(Fe^{III}) activated H₂O₂ to produce •OH and hemin(Fe^{IV}=O). The reactions in Eqs 1-6 greatly promoted the generation of •OH and hemin(Fe^{IV}=O), leading to the extremely rate acceleration of substrates oxidative transformation in the hemin-ACF/AA/H₂O₂ system (Eqs 7 and 8).

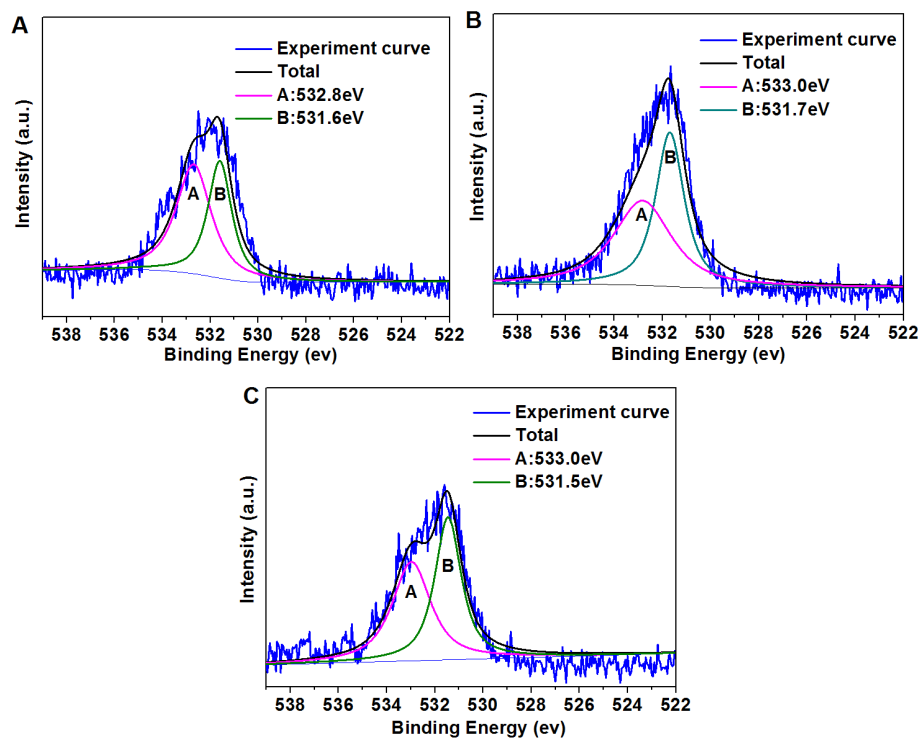
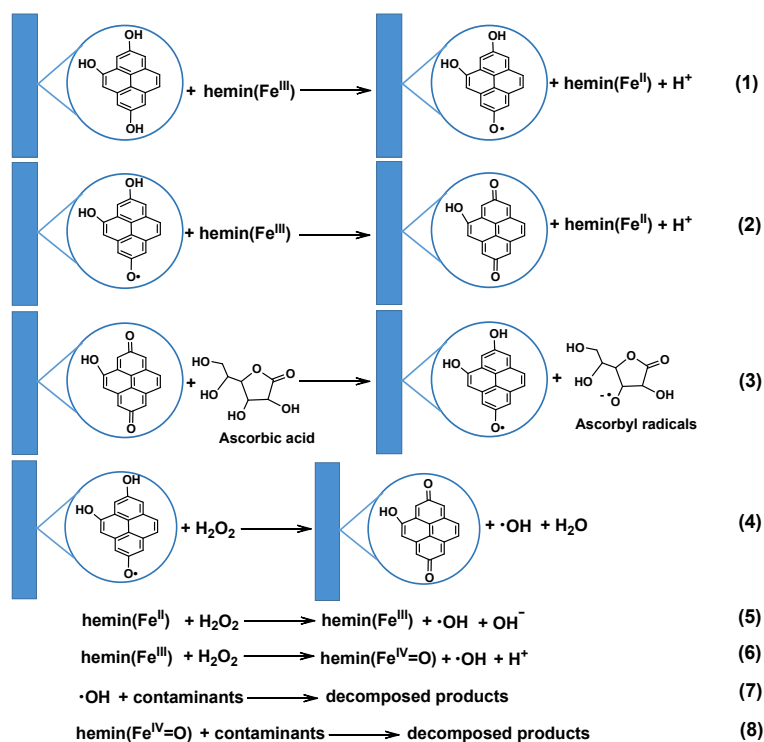


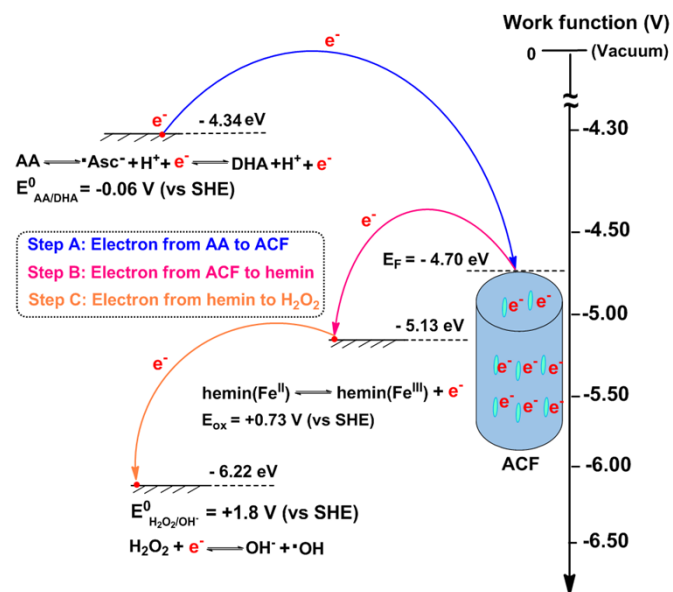
Fig. S21. XPS spectra of O 1s on (A) fresh hemin-ACF, (B) recycle hemin-ACF in the hemin-ACF/H₂O₂ system, and (C) recycle hemin-ACF in the hemin-ACF/AA/H₂O₂ system.



Scheme S1. The proposed mechanisms of contaminants decomposition in the hemin-ACF/AA/H₂O₂ system.

Mechanism for extremely enhanced decomposition from the perspective of electrochemistry.

The electron transfer behavior among AA, ACF and hemin may be beneficial for the promoted catalytic performance. Scheme S2 presents a schematic explanation to this enhancement of activity. The work function of π -conjugated structural carbon material, ACF could be determined to be approximately 4.7 eV, which was related to the Fermi energy (E_F).¹⁷ The oxidation potential of hemin (E_{ox}) was +0.97 V.¹⁸ In addition, the HOMO level of hemin (E_{HOMO} (hemin)) was -5.37 eV based on the empirical formula $E_{HOMO} = -e (E_{ox} + 4.4)$ (eV).¹⁹ This potential difference enabled electron transfer for reduction of hemin(Fe^{III}) to hemin(Fe^{II}). In the hemin-ACF/ H_2O_2 system, the high reduction potential (+1.8 V vs. SHE)²⁰ enabled H_2O_2 to oxidize hemin(Fe^{II}) to hemin(Fe^{III}) via axial coordination between H_2O_2 and the central iron ion, while the H_2O_2 was reduced to $\bullet OH$ (oxidation potential: 2.8 V).²¹ Finally, after losing electrons, the ACF could be rapidly reduced by AA (oxidation potential: 0.06 V),²² resulting in the generation of $\bullet Asc^-$. These reaction steps can be continuously driven by the relative potential difference until complete exhaustion of H_2O_2 , as the decomposition of H_2O_2 belongs to a non-equilibrium redox process. Therefore, the excellent and promoted catalytic performance of the hemin-ACF/AA/ H_2O_2 system may arise from a strong electronic interaction among AA, hemin and ACF.



Scheme S2. Schematic illustration of the hemin-ACF/AA/H₂O₂ catalytic system involving electron transfer from low to high electrochemical potential.

References:

- 1 Y. Yao, Y. Mao, Q. Huang, L. Wang, Z. Huang, W. Lu and W. Chen, *J. Hazard. Mater.*, 2014, **264**, 323.
- 2 G. L. Squadrito, R. Cueto, B. Dellinger, W. A. Pryor, *Free Radic. Biol. Med.*, 2001, **31**, 1132.
- 3 Z. Maskos, L. Khachatryan, B. Dellinger, *Energ. Fuel.*, 2008, **22**, 1027.
- 4 L. W. Tian, C. P. Koshland, J. Yano, V. K. Yachandra, I. T. S. Yu, S. C. Lee, D. Lucas, *Energ. Fuel.*, 2009, **23**, 2523.
- 5 X. Yang, X. Xu, J. Xu, Y. Han, *J. Am. Chem. Soc.*, 2013, **135**, 16058.
- 6 S. Pang, J. Jiang, J. Ma, *Environ. Sci. Technol.*, 2011, **45**, 307.
- 7 O. Pestovsky, A. Bakac, *Inorg. Chem.*, 2006, **45**, 814.
- 8 Y. Yao, Y. Mao, Q. Huang, L. Wang, Z. Huang, W. Lu, W. Chen, *J. Hazard. Mater.*, 2014, **264**, 323.
- 9 L. C. C. Leite, O. Augusto, *Arch. Biochem. Biophys.*, 1989, **270**, 560.
- 10 D. M. Stearns, K. D. Courtney, P. H. Giangrande, L. S. Phieffer, K. E. Wetterhahn, *Environ. Health Perspect.*, 1994, **102**, 21.
- 11 D. M. Stearns, K. E. Wetterhahn, *Chem. Res. Toxicol.*, 1994, **7**, 219.
- 12 R. Fu, H. Zeng, Y. Lu, *Carbon*, 1995, **33**, 657.
- 13 S. Chen, H. Zeng, *Carbon*, 2003, **41**, 1265.
- 14 M. Uchida, O. Shinohara, S. Ito, N. Kawasaki, T. Nakamura, S. Tanada, *J. Colloid. Interf. Sci.*, 2000, **224**, 347.
- 15 J. S. Lakind, A. T. Stone, *Geochim. Cosmochim. Acta.*, 1989, **53**, 961.

- 16 G. Fang, J. Gao, C. Liu, D. D. Dionysiou, Y. Wang, D. Zhou, *Environ. Sci. Technol.*, 2014, **48**, 1902.
- 17 S. C. Lim, H. J. Jeong, K. S. Kim, I. B. Lee, D. J. Bae, Y. H. Lee, *Carbon*, 2005, **43**, 2801.
- 18 S. O. Obare, T. Ito, G. J. Meyer, *Environ. Sci. Technol.*, 2005, **39**, 6266.
- 19 F. Huang, L. Hou, H. Wu, X. Wang, H. Shen, W. Cao, W. Yang, Y. Cao, *J. Am. Chem. Soc.*, 2004, **126**, 9845.
- 20 D. R. Lide, *Handbook of Chemistry and Physics, 87th ed.*, CRC press, Boca Raton, 2007, pp. 820-829.
- 21 E. Neyens, J. Baeyens, *J. Hazard. Mater.*, 2003, **98**, 33.
- 22 Y. Lin, C. Liang, *Environ. Sci. Technol.*, 2013, **47**, 3299.